Eur. Phys. J. B **11**, 161–175 (1999)

THE EUROPEAN PHYSICAL JOURNAL B

EDP Sciences

Dichroism in angular resolved VUV-photoemission from the (0001) surfaces of thin Gd and Nd films epitaxially grown on W(110)

G.H. Fecher[1,a], J. Braun[2], N.A. Cherepkov[3], L.V. Chernysheva[4], Th. Jentzsch[1], J. Morais[1], A. Oelsner[1], Ch. Ostertag[1], J. Paul[1], H.Ufer[2], and G.Schönhense[1]

[1] Johannes Gutenberg-Universität, Institut für Physik, 55099 Mainz, Germany
[2] Fachbereich Physik, Universität Osnabrück, 49069 Osnabrück, Germany
[3] State Academy of Aerospace Instrumentation, 190000 St.Petersburg, Russia
[4] A.F.Ioffe Physico-Technical Institute, 194021 St. Petersburg, Russia

Received 21 September 1998

Abstract. We present investigations of the electronic and magnetic structure of the Rare Earth valence states. In particular, we have examined ultra thin films ($\leq$ 10 ML) of the rare earth metals gadolinium and neodymium epitaxially grown on tungsten (110). Various experiments on dichroism in angular resolved photoemission have been performed using circularly as well as linearly polarised light in the VUV-range with photon energies *below* 40 eV. A special emphasis was placed on the investigation of the surface state, which was observed for both Gd and Nd. A very small magnetic splitting of about 25 meV was observed for the surface state of ferromagnetic Gd. A magnetic ordering of a Nd-monolayer on a remanently magnetised Fe-film is observed. Large dichroism effects are found for the surface state as well as the valence bands of paramagnetic Nd. In the latter case, these are used to determine the dispersion of the valence bands. Different numerical approaches are presented, one based on atomic photoionisation theory, another is based on a one-step model of solid state photoemission. Atomic photoionisation theory is used together with three-step calculations to explain the *non-magnetic* circular dichroism observed in the Gd $4f$ emission. The capability of dichroism experiments for resolving details of the electronic structure and for sensitive tests of photoemission calculations is demonstrated.

PACS. 79.60.-i Photoemission and photoelectron spectra – 78.66.-w Optical properties of specific thin films, surfaces, and low-dimensional structures

1 Introduction

The Rare Earth metals and their compounds have stimulated a lot of scientific work due to their very interesting and unique chemical and physical properties [1]. Electronic and magnetic correlation effects [2] are of special interest in work on these materials. The interaction of the localised $4f$-moments with the valence bands leads to strong magnetism and complicated anti-ferromagnetic spin structures (*e.g.* for Nd [3]).

These elements are thus interesting model systems for experiments on dichroism in the angular distribution of photoelectrons. In such an experiment one measures the difference of the differential cross-sections for either exciting with different polarisation of the photons (*e.g.* right and left circularly polarised) or for the excitation with fixed polarisation from initial states with different orientation (*e.g.* magnetisation $+M$ and $-M$). First experiments of this kind have been performed using circularly polarised synchrotron radiation by Schönhense *et al.* for non-magnetic adsorbates and surfaces [4]. This effect (Circular Dichroism in the Angular Distribution of Photoelectrons, CDAD) was predicted theoretically to appear in emission from molecules by Ritchie [5]. Feder has shown for adsorbates that such asymmetries are a spin-independent phenomenon [6]. Later, it was shown by Parzynsky [7] for atoms and by Cherepkov [8,9] for molecules that the CDAD is an effect arising in pure dipole approximation if the system under investigation is oriented or aligned. Baumgarten *et al.* performed first experiments on ferromagnets [10] (Circular Magnetic Dichroism in..., CMDAD). The dichroism is sensitive to structure and symmetry properties, because an alignment or orientation is necessary to observe any effect [4,11,12]. Large CMDAD effects were found by Starke *et al.* for the $4f$-states of Gd, Tb, and TbFe in the soft X-ray range [13]. The usefulness of magnetic dichroism experiments for the investigation of surface magnetism was also shown [13,14]. Magnetic

[a] e-mail: fecher@mail.uni-mainz.de

Table 1. The dichroism-family: various experiments on dichroism in the angular distribution of photoelectrons are possible. The labels follow the suggestions by Venus [18]. $M^{\pm s,\pm p,\pm n}$ are the vectors of the magnetisation (see Fig. 1) and S_i are the Stokes-parameters describing the polarisation of the photons. (The notation of the Stokes parameters is: S_0 := Intensity, S_1 := linearly polarised ($s := \varepsilon_y$ or $p := \varepsilon_x$); S_2 := linearly polarised (RLP := $\varepsilon_x + \varepsilon_y$ or LLP := $\varepsilon_x - \varepsilon_y$); S_3 := circularly polarised (RCP := $\sigma^+ := \varepsilon_x + \mathrm{i}\varepsilon_y$ or LCP := $\sigma^- := \varepsilon_x - \mathrm{i}\varepsilon_y$). $\varepsilon_{x,y}$ are the electric field components for normal incidence.)

	switched	fixed
LDAD	S_1; s → p	geometry
	S_2; RLP → LLP	
CDAD	S_3; RCP → LCP	
SCDAD	S_3; RCP → LCP	spin of the photoelectron
MCDAD	S_3; RCP → LCP	geometry and
MLDAD	S_1; s → p	magnetisation
	S_2; RLP → LLP	$M^{\pm s}$, $M^{\pm p}$, $M^{\pm n}$
CMDAD	$M^{\pm s}$, $M^{\pm p}$, $M^{\pm n}$	S_3 → RCP or LCP
LMDAD		S_1 → s - or p - polarised
		S_2 → RLP or LLP
UMDAD		unpolarized light

dichroism in the angular resolved photoemission with linearly polarised light MLDAD was first observed by Roth *et al.* for Fe core levels and valence bands [15]. Even unpolarised light can be utilised for MDAD experiments [16]. The magnetic linear and circular dichroism in emission from valence bands was studied analytically by Henk *et al.* [17]. In general, the various possible experiments on dichroism in photoemission form a large family as shown in Table 1. They can be classified according to the orientation or alignment of either the photons or the electronic states under investigation (see also [18]). The first group is characterised by a fixed alignment of the states, but no alignment is necessary to observe LDAD. For completeness we included the effect with fixed spin being a consequence of spin polarisation effects observed in photoionisation of atoms [9,19] and solids [6]. The second group is characterised by a fixed orientation of the states. In principle this must not be ferromagnetic effects, an orientation can also be induced by external fields like in experiments on the Zeeman effect. The third group differs from the first two, because here the orientation is changed rather than the photon polarisation. Common to the effects from oriented states is, that they can be observed not only in the angular distribution, but also in the total cross-section, if the UMDAD is excluded. It is worthwhile to note that the particular geometry of each of the experiments is very important.

Thole and van der Laan have given theoretical models for spin dependent and dichroic effects in emission from core-level including many-particle effects [20]. Cherepkov *et al.* developed a general formalism for the dichroism in (atomic) photoemission [21]. This formalism utilises the state-multipoles instead of density matrix formalism [22] to describe the polarisation (orientation and/or alignment) of the electronic states. This theory has already been applied successfully on the magnetic dichroism from core-levels [23], although it is an atomic theory. All such atomic like models can be easily implemented in a three-step photoemission model. Photoelectron diffraction can be included additionally as described by Fecher *et al.* [24,25]. The $4f$-states exhibit binding energies in the range of the valence band states, but their strongly localised nature makes the use of an atomic model feasible. In this work we will put an additional emphasis on the photoemission from the d_{z^2} surface state, which also has a strong atomic character. We will therefore show how far the atomic model can be used to describe at least qualitatively the magnetic and electronic properties of the solid surfaces that are under investigation here.

We also present results from calculations done with a one-step photoemission program developed by Braun [26], Borstel, and co-workers [27]. This program calculates the photoemission from Bloch-wave initial states using a Greens-function method including spin-orbit-interaction. The final states used in these calculations correspond to time-reversed-LEED states. Compared to an usual LEED-state, here the source is replaced by the detector and all vectors corresponding to group velocities of the electron wave field are reversed.

The paper is organised as follows. First we give a description of the experimental setup and the procedure how to obtain clean and well ordered surfaces being essential for the examination of all dichroic measurements. The section on the results and discussion starts with an overview on the observed spectra being followed by the results of the dichroic measurements and their comparison to theoretical models. We begin that section with the discussion of the cross-section of the surface state being one of the outstanding features of the RE(0001) surfaces. Every theoretical description or calculation has to reproduce first the measured intensity, a fact that is most often neglected in comparison between models and experiments on dichroism. The part on the dichroic measurements is than subdivided in such including magnetic or non-magnetic effects.

2 Experimental

The setup of the experiment is schematically drawn in Figure 1: Photons in the energy range from 5 eV to 38 eV were provided by the 6.5m-NI monochromator [28] at the storage ring BESSY in Berlin. Right and left circularly polarised light with a degree of polarisation $P_{\mathrm{circ}} > 90\%$ is accepted 1 mrad above or below the storage ring plane, and linearly polarised (p-polarised) light in the plane. The light impinges within the x-z-plane at an angle of about 45° with respect to the surface normal (*i.e.* the z-axis).

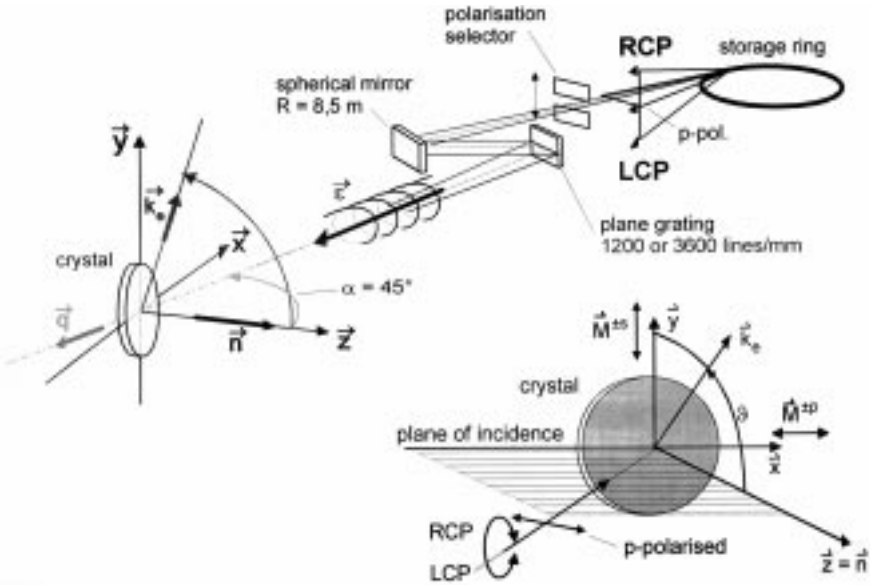

Fig. 1. Setup of the experiment at the 6.5 m normal incidence monochromator at BESSY I (Berlin). The lower right part shows the plane of photon incidence together with the directions of sample magnetisation. $M^{\pm s,\pm p}$ are the possible in-plane components of the magnetisation. (The magnetisation $M^{\pm n}$ parallel to the surface is not shown here.) The angle of light incidence was fixed at about 45° as indicated in the upper part, the observation angle ϑ was variable.

The photoelectrons are detected at an observation angle ϑ (measured with respect to the surface normal) in the x-y-plane perpendicular to the plane of light incidence. The electron energy analyser is of the simulated-hemispherical type with a mean radius of 50 mm. The observation angle ϑ can be varied by a rotation of the spectrometer around the x-axis as described in [29]. The entrance lens system has an angular acceptance better than 1° FWHM. A 90°-deflector similar to the spectrometer guides the electrons back onto the rotational axis, where they are detected by means of a channeltron. The energy resolution of the complete setup (spectrometer and photon source) used in most of the measurements was about 150 meV as determined from the width of the Fermi-edge of photoelectron spectra.

The W(110) single crystal was mounted on a x-y-z-manipulator with rotation around the y and the z-axis (for co-ordinates see Fig. 1). Liquid nitrogen was used to cool the sample to temperatures of about 110 K. The sample holder was equipped with a pair of coils for magnetisation. These coils had a fixed orientation in y-direction being parallel to the W[1$\bar{1}$0]-direction. The structure and the orientation of the sample surfaces was monitored with LEED.

Great care was taken to keep the UHV-system at a base pressure in the low 10^{-11} mbar range, what is a necessary condition for the successful preparation of clean and stable rare earth films. The UHV-system was equipped with a 1500 l/s cryopump additional to a 330 l/s turbo-molecular-pump, a 230 l/s ion getter pump, and a Ti-sublimation pump with a lN_2-cooled baffle.

The tungsten substrate was cleaned by flashing to 2 000-2 300 K. After a larger number of preparation cycles, a beginning contamination with carbon segregating from the bulk could be found, as indicated by characteristic superstructure spots in the LEED-patterns. The C-depletion of the tungsten surface was re-established by heating in O_2 with subsequent flash. In one case, a thin Fe-film grown on the W(110)-crystal served as a remanently magnetiseable substrate for a Nd monolayer (*cf.* [30] and references therein).

The Rare Earth materials were evaporated from a molybdenum crucible by means of an electron beam heated evaporator. Crucible and filament are surrounded by a water-cooled copper shroud which opens into a collimator pipe. The collimator contains an ionisation-gauge like flux monitor (being calibrated by a quartz balance), which allows the reproducible control of growth rates. The film thickness was cross-checked by measuring the intensity of characteristic Auger-lines and MEED-oscillations of the adsorbate *versus* growth time. The crucible was thoroughly degassed prior to loading. The fresh load was melted and degassed in a separate chamber. The evaporator was degassed again after bake-out of the UHV-chamber in order to remove the oxidised surface of the material in the crucible.

Gd and Nd both form hexagonal closed packed crystals (dhcp in the case of Nd) [31]. The direction of growth on the W(110)-surface is along the c-axis ([0001], see *e.g.* [32]). The Rare Earth metals were evaporated on the freshly cleaned substrate. Best results were obtained keeping the substrate at about 100 K during evaporation, with subsequent annealing to 900-1050 K. We observed layer-by-layer growth for the first 2 to 3 monolayers according to [32], monitored by the characteristic edges in the course of the Auger intensities and oscillations observed by MEED. The LEED pattern from 1 ML Gd/W(110) still shows strong W(110)-spots together with a superstructure

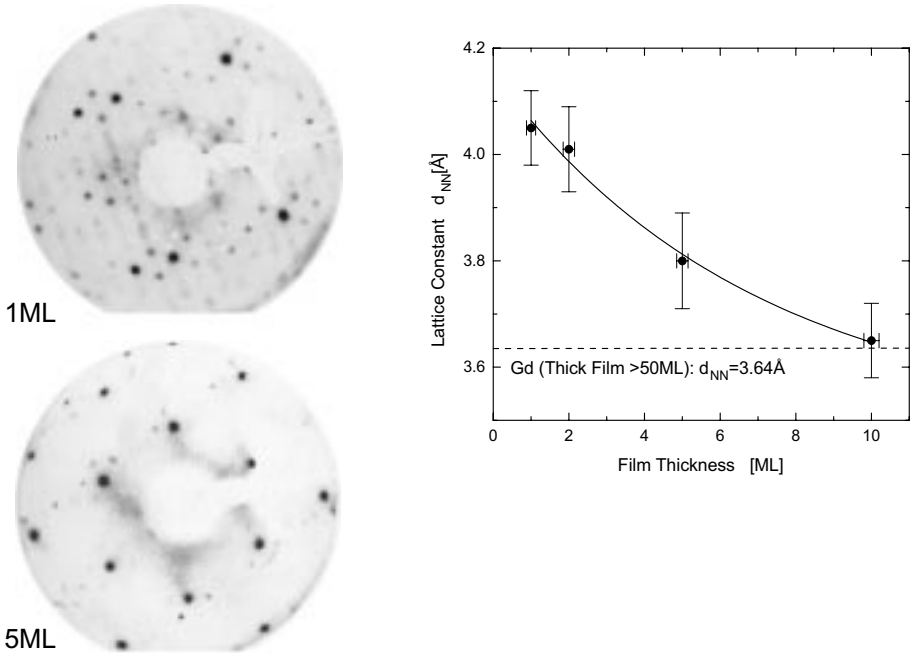

Fig. 2. Crystalline structure of the Gd films. The left part shows LEED patterns taken at 100 eV electron energy after annealing of the films. In the upper part a superstructure with a large period is visible and the W(110)-spots are still dominating at 1 ML. The lower part shows the hexagonal Gd-surface at 5 ML, but a weak superstructure is still visible due to island formation hinting that the Gd(0001) lattice constant is still enlarged by 4% compared to the bulk value. The right part shows the lattice parameter with growing film thickness, the thick film limit is reached at above 10 ML corresponding to about 28.9 Å assuming the bulk lattice parameters.

with high-order coincidence (upper left part of Fig. 2). The lateral lattice constant of the adsorbate decreased with increasing film thickness, approaching the bulk value for a thickness above 10 ML (corresponding to about 28.9 Å if the bulk c-parameter is used) as is shown in the right part of Figure 2. The LEED-pattern of 5 ML Gd/W(110) (lower left part of Fig. 2) shows mainly a hexagonal pattern, with the lattice constant being still enlarged by about 5% compared to the bulk value. The substrate-induced LEED spots are weakened, but still visible. This hints on an island growth mode above 2-3 ML (Stranski-Krastanov-mode), but possibly one can have also a layer by layer growth mode (Frank-van der Merve-mode) with high defect density being closer to Vollmer-Weber-mode. Careful annealing to about 1 000 K led to closed hexagonal surfaces with clear LEED-patterns, that is the surface is smoothened in domains being in size at least as wide as the transfer width of LEED. These observations are in agreement to LEED-IV analysis reported by Giergel *et al.* [33] as well as scanning tunnelling microscopy [34] and spectroscopy [35] investigations of thin Gd films on W(110). It is interesting to note that films grown at room temperature showed a different behaviour. All findings had been similar to that observed for 100 K, but with XPS we detected after annealing an increase of the W lines and in case of films with thickness of about 5 layer and below LEED showed a re-appearence of the W-spots. As far as we did not observe a decrease of any of the rare earth XPS lines, one has to assume a clustering of the films accompanied by uncovering parts of the substrate.

The 10 ML films, as used most often throughout this work, show always the pure hexagonal LEED pattern as reported for bulk materials (see [36] and references there). The quality and cleanness of the films was indicated by the occurrence of the sharp and strong peak in the photoelectron spectra assigned to the surface state. The upper part of Figure 3 shows a spectrum taken from Gd(0001) in normal emission at 32 eV photon energy. The emission from the $4f$ states and from the surface state is clearly visible. No structures are present around 6 eV and 4 eV below the Fermi-level, indicating that the film is free from oxygen or hydrogen contamination. The binding energies in these and all following spectra are always given with respect to the Fermi-energy ε_{F}. The lower part of Figure 3 shows a pair of spectra from Nd, taken before and after annealing. All structures are substantially sharpened after annealing according to the increased structural quality. The $4f$-derived peak has lower intensity on the low energy side. This was also observed in XPS spectra (not shown here) and indicates a reduction of the number of different lattice sites due to closing of gaps in the film by annealing. In particular, for both materials the surface state is clearly visible and can be used as a monitor for the good quality of the films.

3 Results and discussion

Our measurements have been done in the range of photon energies from 12 eV to 38 eV. We will first have a

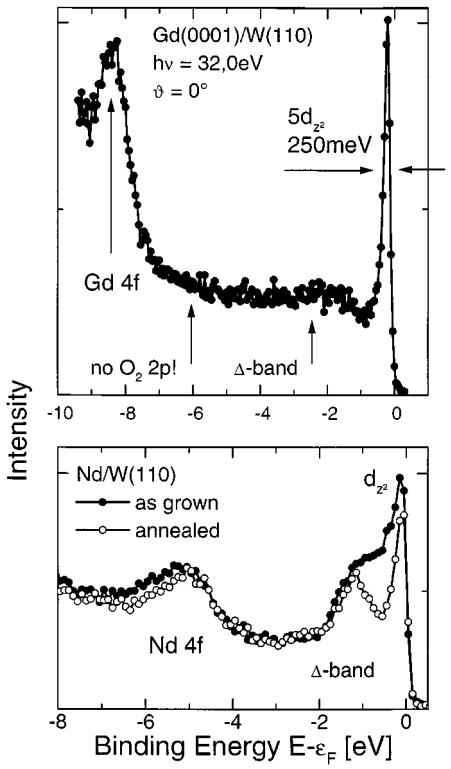

Fig. 3. Upper part: UPS from 10 ML Gd/W(110). The d_{z^2} surface state just below the Fermi-energy is very sharp and dominates the spectrum. Lower part: UPS from 10ML Nd/W(110) before/after annealing. Note that the surface state and valence band emission peaks are sharpened after annealing. The $4f$-derived peak has lower intensity at the low kinetic energy side. (The binding energies in these and all following spectra are given with respect to the Fermi-energy.).

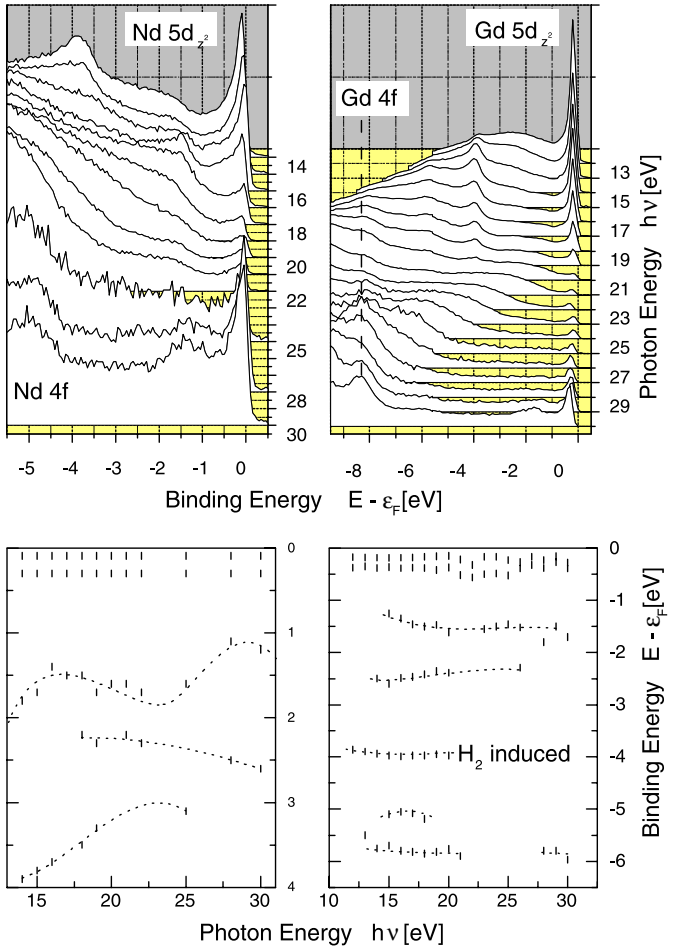

Fig. 4. Upper part: series of UPS-spectra depending on the photon energy from 10ML thick films of Nd(0001) at the left and Gd(0001) on the right. (Gd: p-polarised light, Nd: nominally *unpolarised* light, $I = I^{\mathrm{RCP}} + I^{\mathrm{LCP}}$). All spectra are taken in normal emission. Lower part: dispersion of the observed states and bands. The normal emission direction is parallel to [0001] and corresponds to the Δ-direction of the bulk Brillouin-zone.

look on the general shape of the UPS-spectra at those photon energies. Figure 4 shows series of spectra from Nd (left panel) and Gd (right panel), taken in normal emission at an angle of light incidence of 50°. The Gd-spectra were taken with linearly (p) polarised light, whereas for Nd the sum intensities for excitation with right and left circularly polarised light are given, corresponding to quasi unpolarised light with a small p-component.

The main feature in both series of spectra is a sharp, dispersionless structure just below the Fermi-energy, which can be assigned to emission from the $5d_{z^2}$ surface state. In contrast, the $4f$-derived structures are rather weak and clearly visible only at photon energies above roughly 25 eV. The peak maxima were found at binding energies of $E_{\mathrm{B}} = -4.9 \pm 0.1$ eV for Nd and $E_{\mathrm{B}} = -8.5 \pm 0.1$ eV for Gd. The comparison with values given in the literature [37] shows, that one has a dominant contribution from surface-core-level-shifted states. Only weak and broad structures arise from valence band photoemission. Those bands have predominant d-character, but they are as usual filled by delocalised electrons, that are the two $6s$ and one of the $4f$ ($5d$ in case of Gd) electrons of the free atom being "ionised" to RE^{3+} in the metal. The valence bands are hardly distinguishable from the secondaries in the case of Gd, where in turn the surface state is much more pronounced. In contrast, we found in the case of Nd a stronger emission from the valence band compared to the surface state. Comparing Gd and Nd single atoms, one finds that only Gd has an occupied $5d$ state. Obviously the probability for the occupation of the $5d_{z^2}$ surface state is much higher in this case.

The valence bands are clearly visible for Nd. In principle, a band-mapping along the Δ-direction of the hexagonal Brillouin zone is thus possible. The dispersion of the clearly distinguishable states with photon energy is shown in the lower part of Figure 4. A complete k-mapping needs the final state bands that are only for Gd at low energies available. On the other hand, band structure calculations [38,39] exhibit a huge number of narrow lying occupied as well as unoccupied bands, so that an unambiguous assignment of initial and final state bands (and

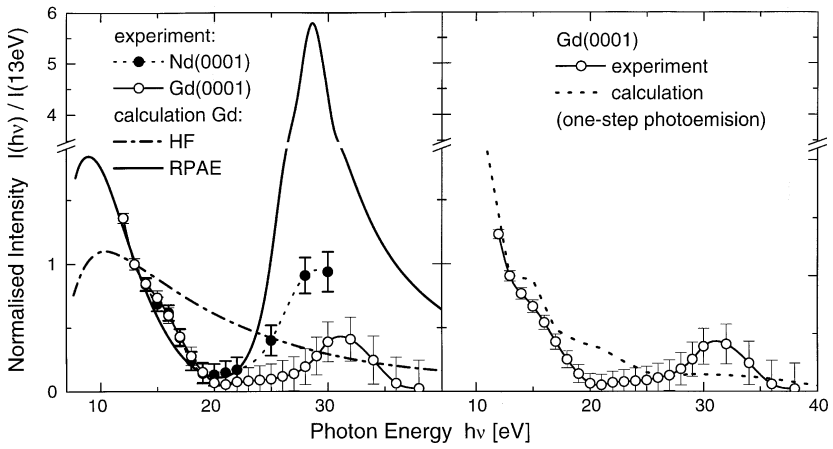

Fig. 5. Dependence of photoemission intensities from the surface states of Gd and Nd on the photon energy, compared with calculations within an one-step-model of solid-state photoemission (right panel) and for atomic photoionisation (left panel).

thus the determination of the location of the transition in k-space) is nearly impossible at the present stage.

The Gd-spectra for lower photon energies exhibit two dispersionless features at $E_B = -3.9 \pm 0.1$ eV and $E_B = -5.7 \pm 0.2$ eV that point on hydrogen adsorption from the residual gas [40]. A polarisation dependent analysis of the H induced states on thin Gd films was recently given by Getzlaff *et al.* [41]. Here, it was accidentally produced by using the Ti-sublimator. This is a small and negligible contamination, since the surface state is not affected. The hydrogen induced states can be removed without changing any other of the observed states by a slight anneal to 700 K. By exposing the Gd film to 2L H_2, we found that at such low exposure neither the width nor the height of the surface state is influenced, even so the height of the H_2 induced state was half of the surface state intensity. Therefore, we conclude that the hydrogen is absorbed by the bulk rather than sitting on top of the surface, at least in the low exposure range. This hypothesis is enforced by the fact, that the same amount of oxygen suppresses the surface state completely, as we have proven in our experiments. All dichroism measurements reported below have been made on H and O free surfaces.

3.1 VUV-photoemission cross sections of the surface state

The most striking feature of both series of spectra is the strong dependence of the cross-section of the surface state photoemission on the photon energy. The intensities are taken from the peak maxima after comparing the secondary electron background and normalisation to the photon intensity. They are shown in Figure 5 for both species, scaled to the value at $h\nu = 13$ eV. Both data sets show a minimum at $h\nu = 20 \pm 1$ eV. A resonance-like maximum at 32 eV $\pm$ 1 eV was found in the case of Gd, where data were taken up to 38 eV. The error in the intensities is mostly determined by the normalisation of the spectra, but the general course was equal in any case. It can not be explained by the monochromator characteristics [28] that was taken carefully into account (please note that the monochromator has a maximum at energies where we observe a minimum in intensity).

In order to explain the experimental findings, we performed calculations for the photoemission from the surface state. The results are compared with the experimental data in Figure 5. The left panel shows results from calculations of the atomic photoionisation, and in the right panel the result from a one-step solid state photoemission calculation is given. The program used in the latter case contains a description of the surface potential barrier after Malmström and Rundgren [42]. It gives only the direct photoemission into a "time-reversed-LEED" final state, but does not regard secondary excitations like Auger-electrons, autoionisation, and other inelastic scattering processes. The result shows a monotone decrease of the cross-sections from lower to higher photon energies, as one would expect for a d-state. The minimum at 20 eV and the maximum at 32 eV are not reproduced. Similar d_{z^2} surface states were also found in calculations for several other (0001)-surfaces of transitions metals, thus seeming to be a common feature of hcp(0001) metal surfaces.

Performing calculations of the electronic density of states, Wu *et al.* [43] found a charge distribution at the surface of Gd, that has the shape of an atomic d_{z^2}-state with some distortion arising from a shift of the charge density into the surface (Fig. 5 in [43]). This charge distribution can be described more exactly by an expansion in terms of Y_{l0}-functions, leading in the simplest case to a distribution of the kind $\sqrt{1-x}d_{z^2} + \sqrt{x}f_{z^3}$, with x being the (small) amount of the spherical harmonic with higher orbital angular momentum. These findings motivated us to treat the surface state in a first approximation as an atomic 5d-state. Thus it was possible to apply the general formalism for angular resolved photoemission (and dichroism in photoemission) developed by Cherepkov and co-workers [21]. Additionally, this atomic model has the advantage that secondary effects like autoionisation can

be included. This feature is not yet available for the one-step calculations.

The dashed line in the left panel was calculated for a single atom in pure Hartree-Fock approximation for the transition $5d \rightarrow \varepsilon f$. A monotone decrease of the cross-sections was found as for the one-step calculation. The result is completely different, if one includes autoionisation: The solid line shows a calculation including an autoionisation-resonance of the type $5p^6 5d^1 \rightarrow 5p^5 5d^2 \rightarrow 5p^6 5d^0$. The electronic correlation is modelled within the Random Phase Approximation with Exchange (RPAE) [44]. This leads to a very strong resonant feature at $h\nu = 28.5$ eV, and to a minimum of the cross-sections that qualitatively corresponds to the minimum observed in the experiments. A similar resonance mechanism was proposed by LaGraffe and Dowben *et al.* [37], who observed the photoemission from Gd(0001) from $h\nu = 20$ eV to 50 eV. They observed a maximum of the photoelectron intensities from the valence band below the Fermi-energy at about 33 eV photon energy. The surface state was not clearly resolved in that work. A similar resonant behaviour for the surface state of Tb(0001) was reported by Wu *et al.* [39] with the maximum at $h\nu = 36 \pm 2$ eV.

The one-step calculation exhibits some modulation of the monotone decrease of the intensity, that is not found in the case of the Hartree-Fock calculation. A three-step calculation including photoelectron diffraction as described in [24], but not including the resonance, showed the same features. These are thus most likely due to photoelectron diffraction.

3.2 Magnetic dichroism in the angular distribution of photoelectrons

We will give some case studies out of the large family of dichroism experiments in angular resolved photoemission, starting with magnetic effects.

3.2.1 CMDAD from Nd/Fe/W(110)

Figure 6 shows results of the magnetic dichroism with circularly polarised light (CMDAD) from a disordered monolayer of Nd on a thin Fe-film (10 layer) grown on W(110). Fe was chosen as a remanently magnetiseable substrate, and Nd is paramagnetic at room temperature. Figure 6 shows pairs of spectra from Nd/Fe/W(110) taken with the magnetisation $M^{\pm s}$ (perpendicular to the plane of light incidence and parallel to the sample surface, see also Fig. 1). The spectra in the left and the right panel were taken with LCP and RCP light, respectively. Additionally, the corresponding difference spectra $I^{M+} - I^{M-}$ are shown. The observation angle was $\vartheta = 30°$. The dominant structure in the spectra is the emission from the Nd $4f$ state at $E_B = -4.7 \pm 0.1$ eV. The weaker features just below the Fermi-energy are most likely due to emission from the iron d-bands. The iron d-band emission appeared to be strongly damped compared to clean Fe, indicating an unusual low mean free path for the electrons penetrating the Nd-monolayer. No dichroism can be distinguished for

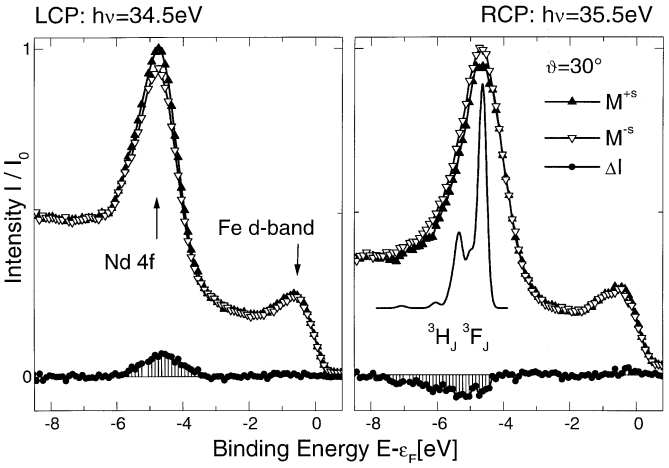

Fig. 6. CMDAD from 1 ML Nd on a remanently magnetised Fe-layer on W(110). Excitation with LCP (left panel) and RCP (right panel) light. The intensities for $M^{\pm s}$ and the corresponding intensity differences are shown. An intensity asymmetry in the $4f$-emission that changes its sign upon changing the helicity of the light is clearly visible, indicating an orientation of the Nd $4f$-states in the magnetic field of the substrate. The right part shows additionally the total intensity for unpolarised light and paramagnetic sample. The lines calculated with Cowans program [45] are broadened by the experimental resolution.

the Fe d-bands (*cf.*, *e.g.* [30]) due to the low intensity. In contrast, the Nd $4f$ emission shows a clear dependence on the orientation of the magnetisation. The photon energy is not exactly the same for both panels, but the difference is too small to affect the photoemission parameters. The effect changes its sign upon changing the sign of the helicity of the light. The effect is not exactly anti-symmetric with respect to the reversal of the polarisation of the light. This is expected from the theory for the case of combined CDAD and CMDAD.

The right part of Figure 6 shows additionally the partial cross-section as calculated by Cowan's program [45]. The final-state fine-structure of the Nd $4f$-peak [46] belonging to the ^3F and ^3H final ionic states was not resolved, also a fine-structure in the dichroism spectrum could not be found for the experimental parameters used here. This is mainly due to the observation from an disordered overlayer.

The CMDAD reveals an orientation of the Nd $4f$-states in the magnetic field of the substrate, which is reversed by changing the sign of the magnetisation. That means that a ferromagnetic order is induced within the Nd adlayer. If an anti-ferromagnetic order were present within the Nd layer, the reversal of the magnetisation would give no observable macroscopic effect: Consider Nd^{3+} with a $^4I_{9/2}$ ground state. Using the notation $|J, M_J\rangle$ one has in the ferromagnetic case $|9/2, -9/2\rangle$ for magnetisation M^+ and $|9/2, 9/2\rangle$ for M^-. In the anti-ferromagnetic case one has always both states $|J, M_J\rangle = |9/2, \pm 9/2\rangle$ equally occupied, and the alignment of the states is not changed by reversing the substrate magnetisation. This approach will not change using the multiplets of the final ionic states.

The matter will become more complicated, if states with $|M_J| \neq J$ are occupied depending on the temperature. Furthermore, the question whether the orientation of the magnetic order in the Nd layer is parallel or antiparallel with respect to the magnetisation of the Fe layer cannot be answered here directly. But, an antiparallel coupling follows from the spin-dependent photoemission results reported by Carbonne *et al.* [47].

The photoelectrons excited with circularly polarised light are spin polarised in general. Thus the observed intensity differences could also be induced by a spin dependent reflection of the photoelectrons at the ferromagnetic substrate. But this contribution to the photo current can be neglected here because of the short mean free path of the electrons in the Nd layer, as was already mentioned: the signal from the iron d-bands is almost completely quenched.

3.2.2 LMDAD from the Gd 4f-state

Here we present results for LMDAD from Gd in the VUV-range. The general shape of the photoelectron spectra for the excitation with photon energies below 40 eV was shown above (Fig. 4). A substantial cross-section for the $4f$-emission was found only for $h\nu > 25$ eV. Figure 7 shows spectra from the Gd $4f$-state taken with p-polarised light at $h\nu = 32$ eV (for geometry see Fig. 1). Each panel shows a pair of spectra for magnetisation up and down together with the difference spectrum, *i.e.* the LMDAD. Two different orientations of the sample magnetisation have been investigated, namely perpendicular ($M^{\pm s}$, upper panel) and parallel ($M^{\pm p}$, lower panels) to the plane of light incidence. (The coils were fixed to the rotatable sample holder, so that the orientation of the magnetisation was always parallel to the W[1$\bar{1}$0]-direction, that corresponds to the $\overline{\Sigma}$ direction of the Gd(0001) surface Brillouin zone.) The photoelectrons were detected in normal e mission in the case of $M^{\pm s}$, whereas for $M^{\pm p}$ the observation angle was $\pm 15°$ with respect to the surface normal.

In all cases, the difference spectra exhibit a small, but clear effect with a change of sign at a binding energy near the peak centre. The lower panels show the reversion of the sign of the effect, if the sign of the observation angle is changed. According to the excitation from a $^8S_{7/2}$ ground state into a multiplet of ^7F_J final states, one has to deconvolute the observed $4f$-peak into a 7-fold multiplet (strictly speaking into two multiplets: one for the bulk contribution, and one with surface-core-level-shift, which is dominant here) [13]. In Table 2 we have given the binding energies of the multiplet for LS and jj coupling as calculated using Cowan's program [45]. This fine structure could not be resolved here. The splitting of two neighbouring lines is expected from the calculations to amount to about 100 meV. Taking into account a lifetime broadening [48] it will be hard to resolve the structure, even using higher resolution. On the other hand we will show below that CDAD measurements hint clearly that we observe only the surface contribution, whereas the bulk

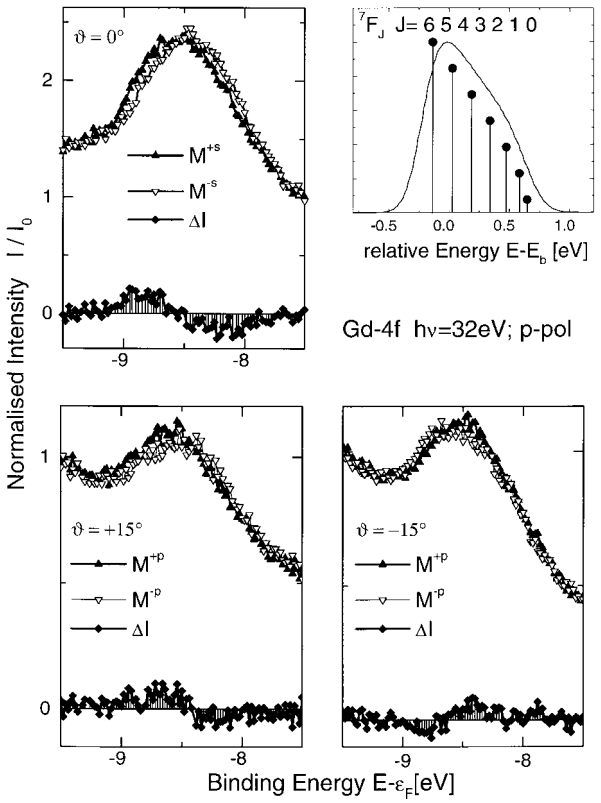

Fig. 7. LMDAD from the Gd $4f$-multiplet for $M^{\pm s}$ (upper left panel) and $M^{\pm p}$ (lower panels). A LMDAD in normal emission was found for $M^{\pm s}$, whereas for $M^{\pm p}$ off-normal emission is necessary, as was expected from the theory. The temperature of the 10 ML thick film was 110 ± 10 K. The upper right part shows the total cross section of the ionic final state ^7F_J multiplet for unpolarised light as calculated using Cowans program [45]. The lines are convoluted by Gausians accounting for lifetime broadening and the experimental resolution.

contribution is completely suppressed at the particular photon energy used in this study.

A complete calculation for the LMDAD from the Gd $4f$-state in terms of the atomic model shown above will be rather complicated (compared to, *e.g.*, the case of Fe-core-levels [23]), because the $4f$-shell is only partially filled. Nevertheless, the angular distribution is mainly described by the single electron equations taking into account the appropriate coupling case (for details of such calculations, see Thole, v.d.Laan *et al.* [20,49]). One has to calculate the partition numbers $n(j, m_j)$ giving the probability that a state $|j, m_j\rangle$ contributes to the emission into a final $^{2S+1}L_J$ multiplet or its jj coupled correspondent, and weight the single electron intensities by the partition numbers as given in Table 2. To get some basic symmetry conditions, one can consider the general equation (17) from [21] which, for our specific geometry ($\mathbf{k} \perp \mathbf{n}$) and neglecting the state multipoles higher than $\rho^{\mathbf{n}}_{30}$ can be

Table 2. Relative binding energies (E_b) of the ionic final state ^7F_J multiplet and single electron partition numbers $n(m)$ for emission from the Gd-4f state. The upper part is for jj and the lower part for LS coupling. The partition numbers n_m are given for M_J with respect to the magnetisation. For arbitrary magnetisation one has to take a rotation of the single particle states into account, what can be established by use of Wigner rotational matrices. In the paramagnetic phase all partition numbers are equal for a given l or j because their is no preferential z-direction, they are given as N. The relative binding energies $E_\mathrm{b} = E_J - E_{4f}$ have been calculated using Cowan's program [45]. The binding energy of the $(7/2, 7/2)_7$ line is far outside of the observed multiplet and therefore omitted.

$^8S_{7/2} \Rightarrow (7/2,j)_J$		n(m$_j$) if M$_J$=-J								N	ΔE$_b$ (^{7}F$_J$) [eV]
	m$_j$=	-7/2	-5/2	-3/2	-1/2	1/2	3/2	5/2	7/2		
J=7	j=7/2	1	1/2	3/13	5/52	5/143	3/286	1/429	1/3432	15/8	
6			1/2	1/2	15/44	2/11	5/66	1/44	1/264	13/8	-0.286
5				7/26	21/52	14/39	35/156	5/52	7/312	11/8	-0.097
4					7/44	7/22	15/44	5/22	7/88	9/8	0.37
3						7/66	35/132	7/22	49/264	7/8	0.188
2							1/12	1/4	7/24	5/8	0.324
1								1/12	7/24	3/8	0.433
0									1/8	1/8	0.497
J=6	j=5/2		1	5/12	5/33	1/22	1/99	1/792		13/6	-0.286
5				7/12	7/15	7/30	7/90	1/72		11/6	-0.097
4					21/55	189/440	27/110	3/44		3/2	0.37
3						7/24	7/18	7/36		7/6	0.188
2							5/18	25/72		5/6	0.324
1								3/8		1/2	0.433
$^8S_{7/2} \Rightarrow {}^7F_J$		n(m$_l$) if M$_J$=-J									
S=3	m$_l$=	-3	-2	-1	0	1	2	3			
J=6	l=3	7/8	7/16	35/176	7/88	7/264	7/1056	1/1056		13/7	-0.301
5			7/16	7/16	7/24	7/48	5/96	1/96		11/7	-0.098
4				21/88	63/176	27/88	15/88	9/176		9/7	0.070
3					7/48	7/24	7/24	7/48		1	0.205
2						5/48	25/96	25/96		5/7	0.270
1							3/32	9/32		3/7	0.373
0								1/8		1/7	0.407

rewritten as

$$I_j^{\mathrm{LMDAD}}(\mathbf{k},\mathbf{n}) = I_j(\mathbf{k},\mathbf{n}) - I_j(\mathbf{k},-\mathbf{n}) = -\frac{\sqrt{2j+1}}{4\pi} 3i\sigma_{nlj}(\omega)(\mathbf{k}\cdot\mathbf{e})(\mathbf{e}\cdot[\mathbf{k}\times\mathbf{n}]) \times \left[\rho^{\mathbf{n}}_{30} C^j_{221} + \frac{1}{2}\rho^{\mathbf{n}}_{30}\left(C^j_{223} - \frac{\sqrt{10}}{2} C^j_{243}\right)\right]. \quad (1)$$

The vectors $\mathbf{k}$, $\mathbf{n}$, and $\mathbf{e}$ are the unity vectors for the directions of electron momentum, magnetisation and photon polarisation. Consider first the case of $M^{\pm p}$, *i.e.* $\mathbf{n}$ lies in the plane of light incidence and $\vartheta = 0$, so that all three vectors $\mathbf{k}$, $\mathbf{n}$, and $\mathbf{e}$ are coplanar. Then the product $(\mathbf{e} \cdot [\mathbf{k} \times \mathbf{n}])$ is equal to zero. That means $I^{\mathrm{LMDAD}} \neq 0$ is only observable at a finite observation angle ϑ. $I^{\mathrm{LMDAD}} \neq 0$ *and* normal emission ($\vartheta = 0°$) is possible in contrast for $M^{\pm s}$. These conditions are fulfilled by our experimental results.

3.2.3 LMDAD from the Gd surface state

The large cross-section of the surface state allows a direct spectroscopic access to the magnetic properties of the surface, as it was shown with spin-resolved ARUPS from Gd [50] and spin-resolved IPS for the image-charge states of Ni [52]. The upper panels of Figure 8 show spectra from the surface state taken with $h\nu = 16$ eV (left) and 30 eV (right) in normal emission. Spectra for $M^{\pm s}$ and the corresponding difference spectra are given like in Figure 7. The LMDAD appears as a small splitting of the spectra for $\pm M$ for both photon energies. The splitting of the peak-maxima is only 17 ± 4 meV at $h\nu = 16$ eV

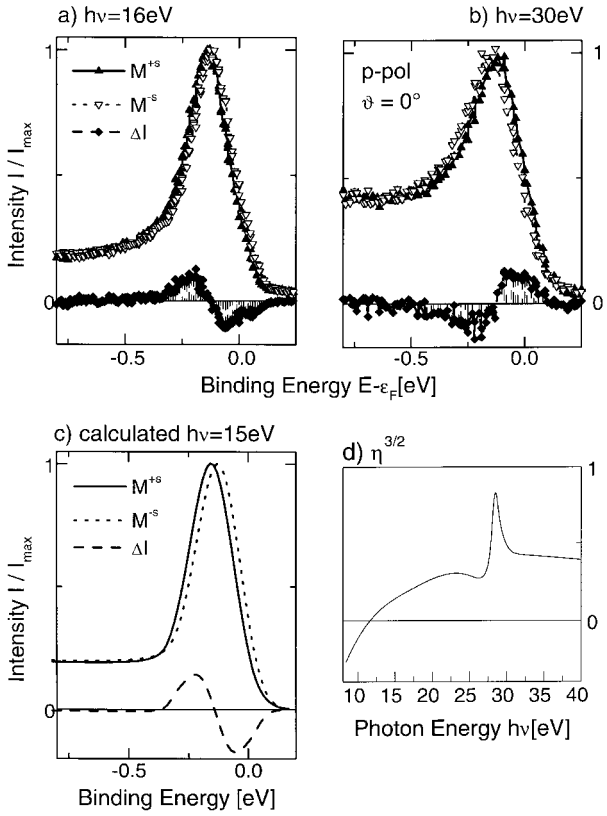

Fig. 8. LMDAD with $M^{\pm s}$ from the Gd surface state. The spectra are taken in normal emission at photon energies below (a, 16.0 eV) and above (b, 30.0 eV) the minimum in the cross-section of the surface state. (c) Calculation of the spectra corresponding to (a) using the one-step-photoemission program. (d) Calculation of the phase-factor $\eta^{3/2}$ within the atomic model depending on the photon energy (see text).

and 28 ± 4 meV at $h\nu = 30$ eV. The course of the difference spectra, *i.e.* I^{LMDAD}, is anti-symmetric with respect to the centre of the emission structure, with a distance of the extreme of 140 ± 10 meV. This can only be explained assuming a splitting of the surface state into at least two substates. The LMDAD has opposite sign for the two different photon energies. The minimum of the cross-section (*cf.* Fig. 5) lies between the chosen photon energies.

To get a qualitative understanding of the observed effects, we used the approximation of an atomic Gd $5d_{3/2}$-state. One would expect then the lifting of the degeneracy with respect to the magnetic quantum number m_j. The observed splitting of the surface state could thereby be explained. Another question remains open: Is the observed reversion of the sign with increasing photon energy connected with the energy dependence of the cross-sections, namely the resonance? Assuming an atomic state, the theory described above is applicable: Consider a $5d_{3/2}$ state and normal emission of the photoelectrons [37]. Then one obtains for the LMDAD

$$I_{3/2}^{\mathrm{LMDAD}} = -\frac{\sigma}{2\pi}\,\frac{6}{\sqrt{5}}\left(\rho_{10}^{n} + \frac{1}{3}\rho_{30}^{n}\right)\eta^{3/2}\sin\alpha, \qquad (2)$$

where α is the angle of light incidence relative to the surface normal, and

$$\eta^{3/2} = -\frac{3}{2}\sqrt{\frac{3}{2}}\,\frac{d_f d_p \sin(\delta_f - \delta_p)}{|d_f|^2 + |d_p|^2}\,. \qquad (3)$$

Here d_f and d_p are the dipole radial matrix elements for excitation into f and p final states and δ their phases. The matrix elements and phases are calculated in the non-relativistic Hartree-Fock approximation with correlation taken into account using RPAE [44,53]. Spin-orbit interaction in the final state leading to $p_{1/2}$ and $p_{3/2}$ partial waves is neglected. The difference in the matrix elements is too small to cause pronounced effects, but results in much more complicated equations. The lower right panel of Figure 8 shows the calculated variation of the parameter $\eta^{3/2}$ with the photon energy. It changes its sign at about 12 eV due to variations of the phase shift difference $(\delta_f - \delta_p)$ between outgoing f and p partial waves. This zero is responsible for the change of sign of the effect. It is obviously not connected with the $5p \rightarrow 5d$ resonance, which produces the sharp feature at 27 eV. The observed zero-crossing is between 16 eV and 30 eV. The difference between theory and experiment can be explained by the difference between the surface state and the $5d$ state of an isolated atom.

The magnitude of the LMDAD is proportional to the sum of state multipoles $\rho_{10}^{n} + \frac{1}{3}\rho_{30}^{n}$ which become $\frac{\sqrt{5}}{3}, 0, 0, -\frac{\sqrt{5}}{3}$ for the sublevels with $m_j = 3/2,\ 1/2,\ -1/2,\ -3/2$, respectively. Thus only the sublevels with $m_j = 3/2$ and $-3/2$ contribute to the LMDAD, and the LMDAD-spectrum consists of a maximum and a minimum of approximately equal magnitudes. This is in agreement with the shape of the observed difference spectra shown in Figure 8.

Furthermore, the one-step photoemission program was applied to calculate the magnetic dichroism. The program is not fully relativistic, thus separate calculations (with separate potentials) are necessary for majority ($\uparrow$) and minority ($\downarrow$) spin, respectively. The surface state is reproduced in the calculations (see above), as well as photoemission from $4f$ derived bands.

Because the computer program does not yet contain a description of resonance processes, we compared the calculations to the experiment only at $h\nu = 16$ eV. The influence of magnetism on the surface state is as follows: One finds different binding energies of the surface state for majority and minority spin. These binding energies are also depending on the width of the surface barrier, which can be tuned with a special parameter in the program. If this parameter (*i.e.* the distance of the turning point of the s shaped profile of the surface barrier to the topmost layer, see above) is chosen equal for both spin channels, the splitting is as big as the width (FWHM) of the measured peak. This is too large, and to get a better agreement with the experiment, one has to chose spin-dependent barrier settings. Indeed, one will find such a shift in a self-consistent calculation of the potential, which will show a difference in the centre of charge for majority and minority electrons near the surface caused by the matching of

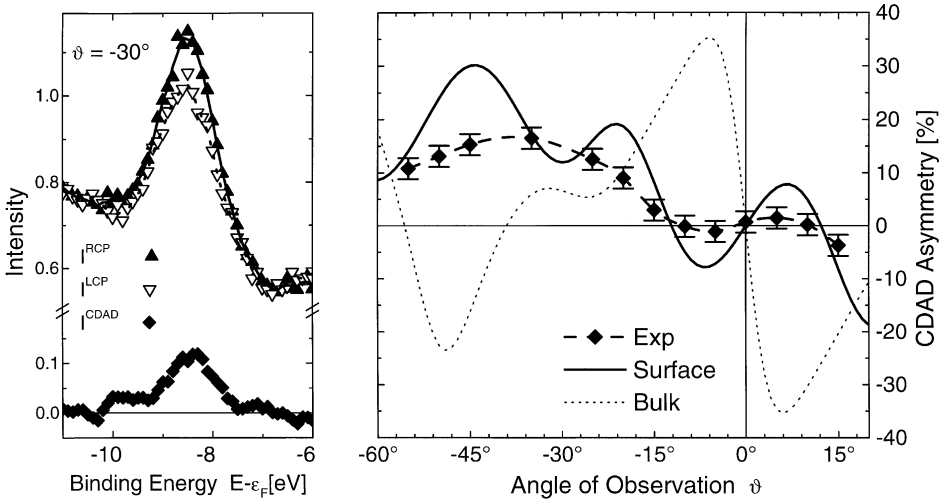

Fig. 9. CDAD from the Gd $4f$ state. Left: photoelectron spectra taken for opposite helicity and the difference $I^{\mathrm{CDAD}} = I^{\mathrm{RCP}} - I^{\mathrm{LCP}}$ on an enlarged scale ($h\nu = 36$ eV, $\alpha = 45°$, $\vartheta = -30°$). Right: CDAD-asymmetry $A_{\mathrm{CDAD}} = \frac{I^{\mathrm{RCP}} - I^{\mathrm{LCP}}}{I^{\mathrm{RCP}} + I^{\mathrm{LCP}}}$ as function of the observation angle. The full drawn line is calculated for the surface and the dotted line for the bulk (sometimes called subsurface) $4f$ state. The calculations account for an incomplete circular polarisation: $P_{\mathrm{circ}} = 0.8$.

the wave-functions in the bulk and in the vacuum. This is essentially the same as a shift of the effective potential for ↑ and ↓ electrons. We tuned the settings of the surface barrier to get a resulting splitting between the majority and minority surface states of 60 meV. This is an average value between the smaller splitting of the spectra for $\pm M$ and the larger splitting of the extrema of I^{LMDAD}. The calculated spectra are convoluted with a Fermi-distribution for $T = 100$ K and a Gaussian corresponding to an overall resolution of the experiment of 150 meV. A secondary electron background after Shirley [51] was added empirically to fit the observed peak-to-background ratio. To be comparable with the experiment, where the photoelectrons are emitted with a spin-polarisation $P < 1$, the majority and minority spectra $I^{\uparrow}$ and $I^{\downarrow}$ had to be mixed to get the intensities I^{M+s} and I^{M-s} for the sample magnetisation M^{+s} and M^{-s}. The best agreement with the measured spectra led to a spin-polarisation of about 64%, which is comparable to results published by Mulhollan *et al.* [50]. Analogous findings have been made for image-charge states of Ni(111) [52]. The turning point of the surface barrier, *i.e.* the measure for its width, was set at 2.4 Å and 2.54 Å measured from the centre of the topmost layer.

This kind of calculation is of course not *ab-initio*, but semi-empirical with a couple of free parameters. Nevertheless, the number of really free parameters can be reduced drastically by using known values from the experiment. By this way we get the model of a surface state in a spin-dependent surface potential, which is consistent with the experiment. On the other hand, this kind of experiments provides a very sensitive test for the photoemission theory.

Recent work on Gd(0001) utilising high resolution photoemission and inverse photoemission [54] and spin-resolved inverse photoemission [55] showed a pure Stoner-like behaviour of the surface state. The exchange splitting reported in both studies for temperatures well below T_{c} and film thickness of 80 Å and 100 Å was about 500 meV. In contrast, our films have been much thinner (see above). The c-axis lattice parameter is possibly still different from its bulk value. This leads to changes in the electronic and magnetic structure: The binding energy of the surface state is shifted compared to the bulk values [54,55], T_{C} is lowered in very thin films, and the easy direction depends on temperature and film thickness [56]. Our results demonstrate the feasibility of the MDAD-technique to resolve even very small exchange splitting as expected near T_{C}.

3.3 CDAD from paramagnetic surfaces

CDAD can be observed already for aligned states [4], so that *no magnetisation* is necessary to observe differences in the angular distribution if the helicity of the photons is changed. In the pure atomic model, the CDAD is merely given by the interference of partial waves differing in the orbital angular momentum l, or the total angular momentum j, respectively. Accounting for solid state effects, especially like photoelectron diffraction, an interference of final state partial waves differing in m_l (or m_j) instead of l will occur, even if initial states from a completely filled shell are investigated [24]. The interference of the $l+1$ and $l-1$ final state partial waves is neglected very often in description of magnetic dichroism in the angular distribution, even so it was demonstrated that it can be of the same order of magnitude as the differential cross section itself.

3.3.1 CDAD from the Gd *4f* state

The results observed from the Gd $4f$ state are shown in Figure 9. The spectra were taken using a photon energy of 36 eV. The left part shows a typical pair of spectra taken at an emission angle of $-30°$ with right and left helicity together with the difference. The difference is positive over the hole energy range of the ^7F_J final state multiplet. We performed 3-step photoemission calculations to estimate the influence from the bulk and surface contribution to the observed CDAD. The results are shown in the right part of Figure 9 together with the measured CDAD asymmetry as function of the angle of emission. The calculation accounting only for the surface part of the $4f$-state reproduces the zero-crossing at about $\pm 12.5°$ very well. (Please note that the asymmetries reproduce only zero-crossings correctly if the photons have an additional linear polarisation, as observed in most experiments.) The observed deviations can be explained by misalignment of the sample or differences in the polarisation delivered by the monochromator. It is clearly seen that one expects the opposite sign for the bulk contribution, even if details of the multiplet structure are not resolved. Therefore we conclude, that at the photon energy used here only the surface contribution is observed, whereas the bulk contribution is completely suppressed. The latter may be due to the fact that the electron mean free path in Gd is much lower than expected from the universal curve.

In our calculations we used LS as well as jj coupling schemes and spin dependent photoelectron diffraction was taken into account. It was found that always the use of jj coupling with $|j, m_j\rangle$ single particle states derived from solution of the Dirac-equation agreed better with the experimental result than the use of LS-coupling with $|l, s\rangle$ electron wave functions, even so the difference of the matrix elements and phases derived from the relativistic Hartree-Fock calculations with Slater-exchange used in the 3-step program amounts only to about 3% for the $l+1$ ($d_{3/2}$ and $d_{5/2}$) partial waves of the emitted electron and was negligible for the g waves. From this we conclude that the coupling is closer to jj than to LS or LSJ, respectively.

The occurrence of asymmetries up to about 17% from the non-magnetic CDAD shows that final state interference cannot be excluded from MCDAD calculations. In future, such calculations should always start from the full relativistic Hamiltonian instead of treating spin-orbit and magnetic-exchange interactions as perturbation.

3.3.2 CDAD from surface states and valence bands

The surface state with its atomic character and large cross-section at low photon energies makes the rare earth surfaces attractive also for the study of the CDAD. Investigations of the surface electronic structure have been performed earlier on Gd(0001) [43,50,57], whereas comparable studies for Nd were not found in the literature.

Figure 10 shows the intensity and the asymmetry A_{CDAD} *versus* $k_{\|}$ of the photoelectrons at $h\nu = 16$ eV.

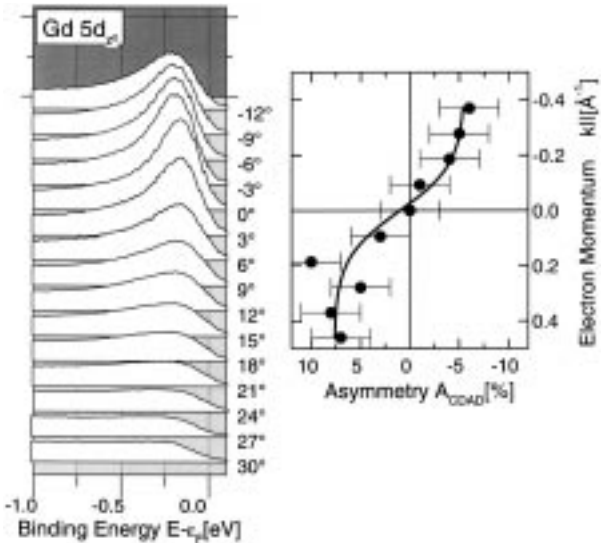

Fig. 10. CDAD from the Gd surface state. Left: photoemission spectra from Gd(0001) taken at 16.0 eV photon energy varying the observation angle ϑ (*unpolarised* light, $I = I^{\mathrm{RCP}} + I^{\mathrm{LCP}}$) Right: the corresponding CDAD-asymmetry *vs.* $k_{\|}$ for Gd.

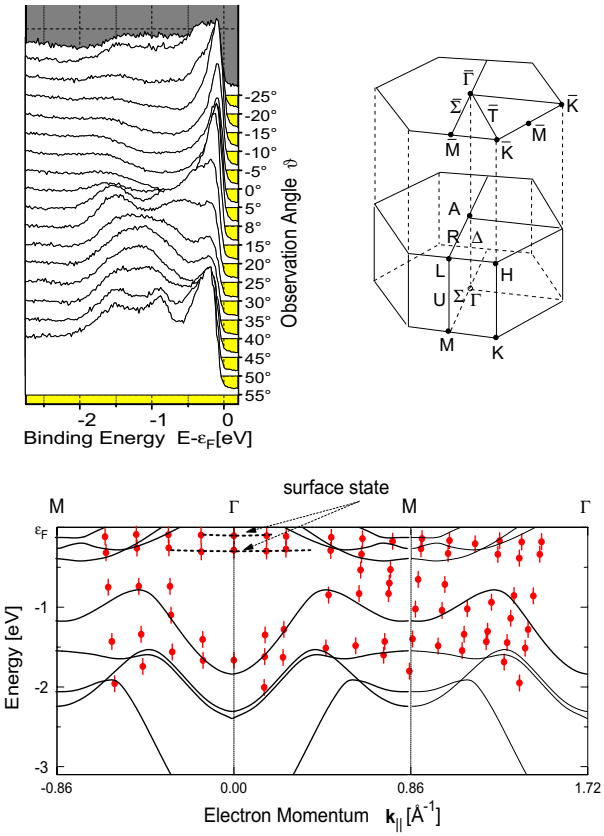

Fig. 11. The upper part shows photoemission spectra from Nd(0001) taken at 16.0 eV photon energy varying the observation angle ϑ in the $\overline{\Sigma}$ direction (unpolarised light, $I = I^{\mathrm{RCP}} + I^{\mathrm{LCP}}$) and the Brioullin-zone of the dhcp crystalline structure. The lower part shows the dispersion of the observed states from Nd(0001) along $\overline{\Sigma}$ as determined from the experiment (bars) compared with a TB-LMTO bandstructure calculation for paramagnetic Nd (lines).

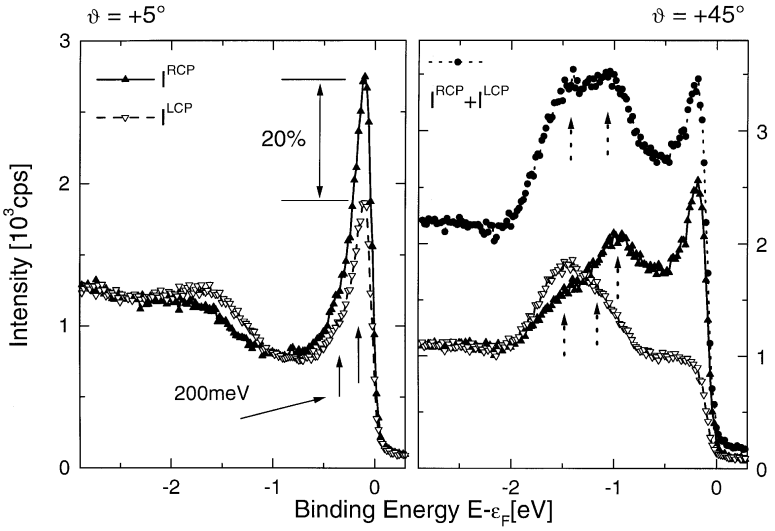

Fig. 12. Photoelectron-spectra from Nd(0001) taken with 16.0 eV photon energy at two different observation angles. Both panels show the intensities for RCP and LCP light. The sum of the RCP and LCP intensities (*unpolarised* light) is additionally given in the right panel.

The plane of observation was within the $\overline{\Sigma}$ direction of the surface Brillouin zone. A rapid decrease of the peak intensity with increasing observation angle ϑ was found. The asymmetry was determined from the peak intensities after background subtraction and is shown in Figure 12, too. An anti-symmetric course with respect to $k_{\|}$ can be seen, with maximum values of about 8%.

We start as before with the consideration of an atomic $5d_{3/2}$ state. The CDAD can then be described by the same formalism as the LMDAD (see above):

$$I_{3/2}^{\mathrm{CDAD}} = -\frac{\sigma}{2\pi}\rho_{20}^{n}\eta^{3/2}\sin\alpha\sin 2\vartheta \qquad (4)$$

with the same parameter $\eta^{3/2}$ as above. In the ferromagnetic case the state-multipoles ρ_{10}^{n} and ρ_{30}^{n} describe the orientation of the different m_j-substates. Here we have only an alignment of the $5d_{3/2}$ state parallel to the surface normal, which is described by ρ_{20}^{n}. The correct sign of the CDAD is given by this model, but an unambiguous fit to the data is not possible because of the limited range of observation angles.

The upper left part of Figure 11 shows a series of photoelectron spectra from Nd(0001) taken at $h\nu = 16.0$ eV and various observation angles from $\vartheta = -25°$ to 55°. The surface state is visible as well as some valence-band features, that are much stronger compared to Gd. A sketch of the experimental geometry is given as well as the hcp Brillouin zone and its projection on the (0001) surface. A clear distinction between the surface state and valence band states crossing the Fermi-edge is possible only in a strongly restricted angular range of $\vartheta = \pm 5°$. As shown in the left panel of Figure 12, a large asymmetry of 20% can be found for this small observation angle. As the CDAD vanishes in normal emission, the variation of the CDAD with the observation angle is very strong here. This can be expected for the case of a d_{z^2}-state, as was shown earlier [11].

The right panel of Figure 12 shows an exemplary set of spectra taken at $\vartheta = 45°$. The spectra taken with RCP and LCP light are given together with the sum, corresponding to unpolarised light. In the latter case one can distinguish a sharp, asymmetric peak just below the Fermi-energy and additionally a broad feature, that seems to consist of two peaks as indicated by the arrows. The spectra taken with circularly polarised light show a strong CDAD, especially at the Fermi-energy. The broad structure at about 0.5 to 2 eV below the Fermi-edge is now resolved into a triple feature. This enhanced resolution was utilised to determine the binding energies of all observed emission features. The corresponding $k_{\|}$-values were calculated taking into account a work function of $\Phi = 3$ eV [58]. The resulting experimental band structure of Nd along the $\overline{\Sigma}$ direction of the surface Brillouin-zone is given in the lower part of Figure 11. The surface state is marked as far as it can be distinguished clearly. The experimental data (bars) are compared with a TB-LMTO (Tight Binding-Linear Muffin Tin Orbitals) calculation (solid lines) for dhcp Nd. The main features of the experimental data are roughly reproduced by the calculation, namely the band gap at the $\overline{\Gamma}$-point, some bands between -1 eV and -2 eV, and the bands just below the Fermi-energy around $\bar{M}$. Some disagreement between theory and experiment was expected however, since the calculation was performed without taking into account $4f$-$5d$ correlation and is thus only a first approximation.

Looking more closely at the surface state (Fig. 12, left panel), one finds a shoulder at the low energy side of the peak. The surface state obviously consists of two states, separated by approximately 200 meV as indicated by the arrows. Recent results for Tb(0001) (not shown here) hint on a similar splitting. The nature of this splitting is clearly not magnetic. Wu *et al.* [39] found a splitting of the surface state of comparable size in calculations for the band-structure of Gd(0001), whereas in our spectra from Gd we cannot unambiguously fit a double peak.

On the other hand, our one-step calculations for Gd and Nd give only a single peak. The surface potential is here modelled by a smooth step function, that depends only on the co-ordinate parallel to the surface normal and is not modulated in directions parallel to the surface. Also the surface potential does not exceed the topmost layer, and no relaxation of the first layers is included. Therefore the splitting must reflect the details of the crystal structure at the surface.

4 Summary and conclusion

We presented an angle resolved photoemission study from epitaxially grown Gd and Nd ultra thin layers on W(110) in the VUV-range. Magnetic and non-magnetic dichroism experiments have been performed on both the $4f$ photoemission and the emission from the surface state. The feasibility of this technique for the investigation of minute details of the electronic structure and magnetic properties was demonstrated: A magnetic coupling of a monolayer of Nd to a ferromagnetic Fe layer has been shown by CMDAD. The surface band structure was determined experimentally for pure Nd(0001). A small, but significant LMDAD was found for the Gd $4f$-states.

One major interest of our work however was put on the investigation of the surface state in both materials: Large cross-sections that strongly increase towards photon energies near the threshold can be found. Thus it is feasible to study the electronic and magnetic properties of the surface by ARUPS-experiments on the surface states. For an ultrathin Gd-film, a LMDAD was found exhibiting a very small splitting of the surface state for the direction of magnetisation lying within the surface. Our results can be explained in terms of an atomic picture by photoemission from oriented m_j-substates. These experimental findings are qualitatively reproduced by the calculations as well as the CDAD from paramagnetic Gd. A better accuracy of the calculations may be achieved including a more exact ansatz for the surface state, where the deviation of the charge distribution of the surface state from a pure d_{z^2}-shape is modelled *via* LCAO or a more sophisticated theory. A second theoretical approach is given by one-step calculations of the solid-state photoemission. It was possible to simulate the observed effect with semi-relativistic calculations including a spin-dependent surface barrier. (Note: a much too large splitting was observed if using a spin *in*dependent barrier.) Nevertheless, the experimental findings show that there is still a rather large discrepancy to the theoretical models.

From the non-magnetic CDAD we found that the total angular momentum of the Gd surface state is of $j = 3/2$ character, as proposed in earlier work [37]. For the $4f$-state we were able to show that at low photon energies the contribution from the surface is dominating, whereas the bulk like state is completely suppressed.

The examples of dichroism experiments in angular resolved photoemission being presented in this work demonstrate that these kinds of experiments provide very sensitive tests of photoemission theories, because more detailed information is gained than in common ARUPS. Details of the electronic structure can be resolved better. This special feature can be used for the investigation of the electronic structure of solid surfaces.

The authors thank the BESSY-staff for good co-operation during the beamtimes. Financial support by the German government (BMBF) is gratefully acknowledged (contract no.: VDI-TZ 13N6609). N.A.C. acknowledges the hospitality of the University of Mainz and financial support by the DFG (SFB 252 TP:F4, and 436 RUS 113/372). G.H.F. is grateful to C.S. Fadley and his group (Lawrence Berkeley Laboratory, Berkeley, CA) and acknowledges financial support by the DAAD.

References

1. *Handbook on the Physics and Chemistry of Rare Earths*, edited by K.A. Gschneidner Jr., L. Eyring (Elsevier, Amsterdam).
2. P. Fulde, J. Phys. F **18**, 601 (1988); G. Zwicknagl, Phys. Bl. **49**, 657 (1993).
3. S.W. Zochowski, K.A. McEwen, E. Fawcett, J. Phys. Cond. Matter **3**, 8079 (1991); K.A. McEwen, S.W. Zochowski, J. Magn. Magn. Mater. **90/91**, 94 (1990); A. Jaroszewicz, P. Kocinski, G. Tecza, Phase Transitions **20**, 195 (1990).
4. C. Westphal, J. Bansmann, M. Getzlaff, G. Schönhense, Phys. Rev. Lett. **63**, 151 (1989); G. Schönhense, Phys. Scr. T **31**, 255 (1990).
5. B. Ritchie, Phys. Rev A **12**, 567 (1975).
6. R. Feder, Solid State Commun. **21**, 1091 (1977).
7. R. Parzynski, Act. Phys. Pol. A **57**, 49 (1980).
8. N.A. Cherepkov, Chem. Phys. Lett. **87**, 344 (1982).
9. N.A. Cherepkov, Adv. At. Mol. Phys. **19**, 395 (1983).
10. L. Baumgarten, C.M. Schneider, H. Petersen, F. Schäfers, J. Kirschner, Phys. Rev. Lett. **65**, 492 (1990).
11. G. Schönhense, Vacuum **41**, 506 (1990).
12. N.A. Cherepkov, V.V. Kuznetsov, Z. Phys. D **7**, 271 (1987); J. Phys. B **22**, L405 (1989).
13. K. Starke, E. Navas, L. Baumgarten, G. Kaindl, Phys. Rev. B **48**, 1329 (1993); K. Starke, L. Baumgarten, E. Arenholz, E. Navas, G. Kaindl, Phys. Rev. B **50**, 1317 (1994).
14. Ch. Ostertag, J. Paul, N.A. Cherepkov, A. Oelsner, G.H. Fecher, G. Schönhense, Surf. Sci. **377-379**, 427 (1997).
15. Ch. Roth, F.U. Hillebrecht, H.B. Rose, E. Kisker, Phys. Rev. Lett. **70**, 3479 (1993).
16. M. Getzlaff, Ch. Ostertag, G.H. Fecher, N.A. Cherepkov, G. Schönhense, Phys. Rev. Lett. **7**, 3030 (1994).
17. J. Henk, T. Scheunemann, S.V. Halilov, R. Feder, J. Phys. Cond. Matter **8**, 47 (1996).
18. D. Venus, Phys. Rev. B **48**, 6144 (1993); Phys. Rev. B **49**, 8821 (1994).
19. U. Fano, Phys. Rev **178**, 131 (1969); **184**, 250 (1969).
20. B.T. Thole, G. van der Laan, Phys. Rev. B **44**, 12424 (1991); Phys. Rev. B **48**, 210 (1993); Phys. Rev. B **49**, 9613 (1994); Phys. Rev. B **52**, 15355 (1995).
21. N.A. Cherepkov, V.V. Kuznetsov, V.A. Verbitskii, J. Phys. B **28**, 1221 (1995).
22. K. Blum, *Density Matrix Theory and Applications* (Plenum Press, New York, 1981).

23. N.A. Cherepkov, Phys. Rev. B **50**, 13813 (1994); G. Rossi, F. Sirotti, N.A. Cherepkov, F. Combet Farnoux, G. Panaccione, Solid State Commun. **90**, 557 (1994).
24. G.H. Fecher, Europhys. Lett. **29**, 605 (1995).
25. G.H. Fecher, A. Oelsner, Ch. Ostertag, G. Schönhense, J. Elec. Spec. Rel. Phen. **76**, 97 (1995); **76**, 289 (1995) A. Oelsner, G.H. Fecher, Ch. Ostertag, Th. Jentzsch, G. Schönhense, Surf. Sci. **331-333**, (1995) 349.
26. J. Braun, Rep. Prog. Phys. **59**, (1996) 1267.
27. G. Thörner, G. Borstel, Phys. Stat. Sol. (b) **126**, 617 (1984); J. Braun, G. Thörner, G. Borstel, Phys. Stat. Sol. (b) **130**, 643 (1985).
28. F. Schäfers, W. Peatman, A. Eyers, Ch. Heckenkamp, G. Schönhense, U. Heinzmann, Rev. Sci. Instrum. **57**, 1032 (1986).
29. G. Schönhense, Appl. Phys. A **41**, 39 (1986).
30. J. Bansmann, M. Getzlaff, Ch. Ostertag, G. Schönhense, Surf. Sci. **352-354**, 123 (1996).
31. R.W.G. Wyckoff, *Crystal Structures*, Vol. 2, 2nd edition (Interscience Publishers, New York, 1964).
32. J. Kolaczkiewicz, E. Bauer, Surf. Sci. **175**, 487 (1986).
33. J. Giergiel, A.W. Pang, H. Hopster, X. Guo, S.Y. Tong, D. Weller, Phys. Rev. B **51**, 10201 (1995).
34. E.D. Tober, R.X. Ynzunza, C. Westphal, C.S. Fadley, Phys. Rev. B **53**, 5444 (1996).
35. R. Pascal, Ch. Zarnitz, M. Bode, R. Wiesendanger, Phys. Rev. B **56**, 3636 (1997).
36. S.D. Barrett, Surf. Sci. Rep. **14**, 271 (1992).
37. P.A. Dowben, D. LaGraffe, M. Onellion, J. Phys. Cond. Matter **1**, 6571 (1989).
38. J. Sticht, J. Kübler, Solid State Commun. **53**, 526 (1985).
39. S.C. Wu, H. Li, Y.S. Li, J. Quinn, F. Jona, Phys. Rev. B **44**, 13720 (1991).
40. D. Li, J. Zhang, P.A. Dowben, M. Onellion, Phys. Rev. B **48**, 210 (1993).
41. M. Getzlaff, M. Bode, R. Wiesendanger, Phys. Rev. B **58**, 9681 (1998).
42. G. Malmström, J. Rundgren, Comp. Phys. Comm. **19**, 263 (1980).
43. R. Wu, C. Li, A.J. Freeman, C.L. Fu, Phys. Rev. B **44**, 9400 (1991).
44. M.Ya. Amusia, N.A. Cherepkov, *Case Stud. Atomic Phys.* **5**, 47 (1975).
45. R.D. Cowan, J. Opt. Soc. Am. **58**, 808 (1968); **58**, 924 (1968).
46. P.A. Cox, J.K. Lang, Y. Baer, J. Phys. F **11**, 113 (1981).
47. C. Carbone, R. Rochow, L. Braicovich, R. Jungblut, T. Kachel, D. Tillmann, E. Kisker, Phys. Rev. B **41**, (1990) 3866.
48. H. Ogasawara, A. Kotani, B.T. Thole, Phys. Rev. B **50**, 12332 (1994).
49. W.J. Lademann, A.K. See, L.E. Klebanoff, G.v.d. Laan, Phys. Rev. B **54**, 17191 (1996); G.v.d. Laan, E. Arenholz, E. Navas, A. Bauer, G. Kaindl, Phys. Rev. B **53**, R5998 (1996); H. Ogasawara, A. Kotani, B.T. Thole, Phys. Rev. B **50**, 12332 (1994).
50. G.A. Mulhollan, K. Garrison, J.L. Erskine, Phys. Rev. Lett. **69**, 3240 (1992).
51. *Practical Surface Analysis by Auger and X-ray Photoelectron Spectroscopy*, edited by D. Briggs, M.P. Seah, (J.Wiley & Sons, Chichester, New York, 1983).
52. M. Donath, Surf. Sci. Rep. **20**, 251 (1994).
53. N.A. Cherepkov, L.V. Chernysheva, Bull. Acad. Sci. USSR, Phys. Ser. **41**, 46 (1977).
54. E. Weschke, C. Schüssler-Langeheine, R. Meier, A.V. Fedorov, K. Starke, F. Hübinger, G. Kaindl, Phys. Rev. Lett. **77**, 3415 (1996).
55. M. Donath, B. Gubanka, F. Passek, Phys. Rev. Lett. **77**, 5138 (1996).
56. G. André, A. Aspelmeier, B. Schulz, M. Farle, K. Baberschke, Surf. Sci. **326**, 275 (1995).
57. F.J. Himpsel, B. Reihl, Phys. Rev. B **28**, 574 (1983).
58. L.P. Zadorozhnyi, V.K. Medvedev, T.P. Smereka, F.M. Gonchar, Sov. Phys. Solid State **34**, 561 (1992).